Structural Changes, Magnetic Properties and Dielectric Behaviour of Tb^{3+} doped Ni-Cd Mixed Ferrites.

Binu P Jacob*, Ayishabi P K, AryaB and Abdul Gafoor M P

Department of Physics, K.M.M. Govt. Women's College, Kannur, Kerala, 670004, India.

*Corresponding Author at: Dept. of Physics, K.M.M. Govt. Women's College
Kannur, Kerala, 670004, India
E-mail address: binupjac@gmail.com
Ph. 919446270667, Fax: 914842363038

Abstract: Terbium Terbium doped Ni-Cd mixed ferrite samples with general formula $Ni_{0.9}Cd_{0.1}Tb_xFe_{2-x}O_4$ (x = 0, 0.02, 0.06 and 0.1) were prepared through sol-gel technique. The effect of terbium doping on the properties of Ni-Cd ferrite has been investigated using different characterization techniques like X-Ray Diffraction (XRD), Fourier Transform Infrared Spectroscopy (FTIR), Wavelength Dispersive X-Ray Fluorescence Spectrometer (WD-XRF), Transmission Electron Microscope (TEM) and Vibrating Sample Magnetometer (VSM). XRD analysis confirmed the formation of single phase spinel structure in all the samples. Tb^{3+} doping is observed to increase the saturation magnetization and resistivity of Ni-Cd mixed ferrite

Key words: sol-gel technique, ferrite, Tb^{3+} substitution, magnetic properties.

1. Introduction

Substitution of rare earth metal ions into the spinel ferrites has been reported to make structural distortions and induce strain and thus significantly modify the electrical and magnetic properties [1]. The addition of rare earth ions to the ferrite system acts as a sintering catalyst that helps in the development of solid solution at lower temperatures [2]. There are many parameters that influence the role of rare earths in the behaviour of ferrites. The most important of them are the electronic configuration, and ionic radii. The rare earth ions are of larger radii to occupy the tetrahedral or the octahedral sites [3]. If their concentrations are high, this leads to the formation of grain boundaries [4]. In addition, the valency of the rare earth ion is of great importance for the compound formation and can explain some of its electrical properties [5]. Only a few reports are available on the properties of rare earth substituted ferrite nanoparticles. The electrical, magnetic and structural properties of rare earth doped nickel ferrite are not well explored

in the nanoregime. Magnetic and dielectric properties of Pr^{3+} doped Ni-Zn mixed ferrites are reported [6]. Kamala Bharathi et al have reported the improvement of both dielectric constant and magnetocapacitance of nanocrystalline nickel ferrite by the substitution of small amount of Gd and Nd ions [7]. Sileo et al. have reported the enhancement of magnetic permeability and lower magnetic losses for nickel ferrite substituted by Gd [8]. The structural and physical properties of nickel ferrite, substituted by Tb^{3+} ions for divalent Ni ions, have been reported [9]. Hence a systematic study on the fundamental properties of rare earth doped nano ferrites may lead to new ideas and the applications of these materials can be extended to more diverse areas. In this paper the effect of rare earth terbium doping on the structural, magnetic and electrical properties of Ni-Cd mixed ferrites is investigated.

2. Experimental

2.1. Synthesis

Terbium substituted Ni-Cd ferrite $Ni_{0.9}Cd_{0.1}Tb_xFe_{2-x}O_4$ (x =0, 0.02, 0.06 and 0.1) were prepared using sol-gel technique. AR grade ferric nitrate, nickel nitrate, cadmium nitrate and terbium nitrate were used as the reagents (99.9% pure MERK). Details of the method are already reported in our previous paper [10]. Each composition obtained was ground well and sintered in a muffle furnace at 400°C for 2 hours. For electrical and dielectric study cylindrical pellets (10mm diameter and 2-3mm thickness) were made using hydraulic press by applying uniform pressure of 5 ton. For porosity measurement, cylindrical disc shaped pellets (diameter=10mm and thickness= 1-2mm) of the samples were made using a hydraulic press by applying a uniform pressure of 5 ton.

2.2. Characterization

The structural characterization of the prepared samples were carried out using BRUKER make AXS D8 ADVANCE powder X-ray diffractometer with Cu-Kα radiation (λ= 1.5406Å) at 40kV and 35mA. Scanning was performed from 20^o to 70^o at a step size of 0.02^o per second for each sample. The crystal structure, lattice constant, crystallite size and X-ray density were determined. Composition of the samples was verified using Wavelength Dispersive X-ray Fluorescence Spectrometer (WD-XRF, BRUKER S4-PIONEER). The Fourier Transform Infrared (FTIR) absorption spectra of the samples were recorded using FTIR Spectrometer (Thermo Nicolet, Avatar 370) in the wave

number range 4000 to 400 cm^{-1} with Potassium bromide (KBr) as solvent. Transmission Electron Microscopy (TEM, Philips CM-10) was used to investigate the morphology and particle size of the synthesized Ni-ferrite samples. Magnetic characterization was carried out using Vibrating Sample Magnetometer (VSM, Lakeshore 7410) at room temperature up to a maximum field of 20kOe. Dielectric properties of the samples were measured using an impedance analyzer (WAYNE KERR 6500B) in the frequency range 100Hz to 20MHZ and in the temperature range 300K to 563K

3. Results and discussion

3.1. Structural analysis

XRD pattern of $Ni_{0.9}Cd_{0.1}Tb_xFe_{2-x}O_4$ (x =0, 0.02, 0.06, 0.1) nanoparticles sintered at 400^oC are shown in figure 1. The pattern was compared with standard data and the formation of single phase cubic spinal structure in all the samples was confirmed.

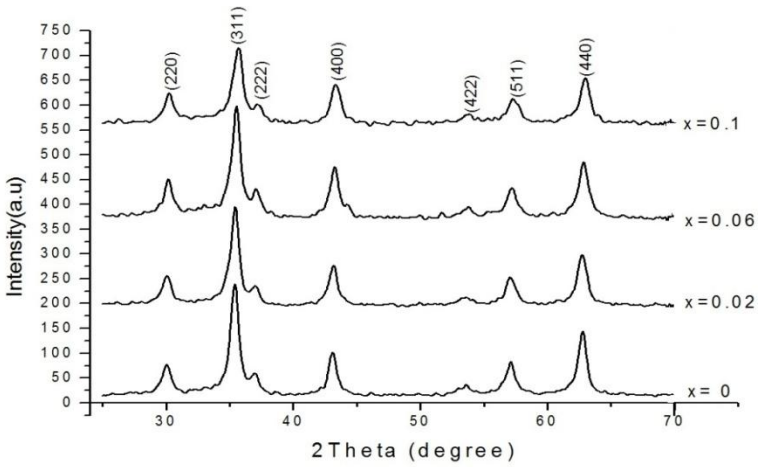

Figure 1. X-ray diffraction patterns of $Ni_{0.9}Cd_{0.1}Tb_xFe_{2-x}O_4$ ferrite system.

Average value of lattice parameter (*a*) of each sample was calculated from inter planar spacing (*d*) values using equation 2.6. The X-ray density of the samples was calculated using the formula [9],

$$\rho_x = \frac{8M}{Na^3} \tag{1}$$

Apparent densities of the samples were determined using the formula,

$$\rho_a = m \big/ \pi r^2 h \tag{2}$$

Where, m is the mass, r is the radius and h is the height of the pellet used. Percentage of porosity was calculated using the formula [11]

$$P = (1 - \frac{\rho_a}{\rho_x}) * 100 \quad (3)$$

Table 1 Structural parameters of Ni-Cd-Tb mixed ferrite system.

Compo-sition x	Lattice parameter a (Å)	Crystallite size (nm)	X-ray density (g/cm^3)	Apparent density (g/cm^3)	Porosity (%)
0.0	8.402	19.3±1.4	5.369	2.789	48.05
0.02	8.389	24.3±0.9	5.504	2.852	48.17
0.06	8.369	25.5±1.1	5.574	2.843	48.99
0.1	8.357	21.8±0.6	5.627	2.857	49.21

The structural parameters of the studied samples are tabulated in table 1. Owing to the large ionic radius of Tb^{3+}, lattice parameter of the samples is expected to increase. However in contradiction to similar reports lattice parameter of Ni-Cd-Tb system is found to decrease with terbium content. E. Melagiriyappa et al [12] have reported a similar decreasing trend in the lattice parameter of Mg-Zn ferrite by samarium doping and was attributed to the occupation of Sm^{3+} ions on octahedral sites. Hence it can be concluded that there may be some other factors like bond length, long range Coulomb attractive force, distribution of cations over tetrahedral and octahedral sites etc., that influence the lattice constant. According to Bragg's equation, increase in diffraction angle means a decrease in lattice constant and vice versa. It can be seen from figure 1 that XRD peaks are shifted a little to the right side for all the samples as expected. The estimated crystallite sizes are in the nanometre range between 18nm and 27nm. Porosity of the samples is observed to increase with terbium content.

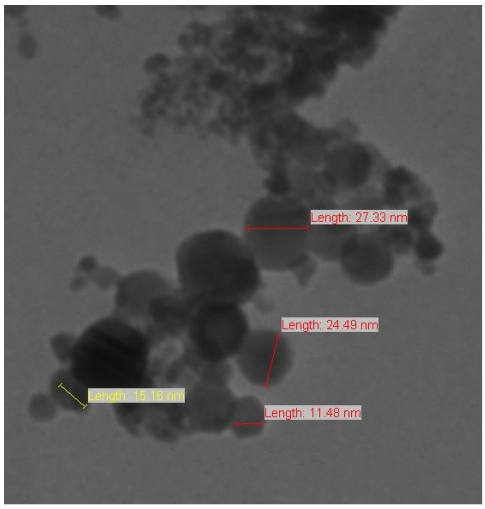

Figure 2. TEM image of $Ni_{0.9}Cd_{0.1}Tb_{0.1}Fe_{1.9}O_4$ nanoparticles.

Various researchers have reported a decrease in crystallite size of ferrite nanoparticles by the doping of rare earth ions [11, 13, 14]; however in the present system of doped nickel cadmium ferrite, crystallite size is observed to increase with Tb^{3+} concentration. The X-ray density increases as a function of Tb^{3+} ion content as it mainly depends on the molecular weight of the sample. The percentage porosity of the samples is found to increase with increase in Tb^{3+} concentration.

Figure 2 shows TEM image of $Ni_{0.9}Cd_{0.1}Tb_{0.1}Fe_{1.9}O_4$ sample. From the image, it is clear that most of the nanoparticles are of almost spherical shape and are agglomerated. Some of the nanoparticles are completely agglomerated and are appearing like big particles in the images. Average particle size obtained from TEM analysis is in the range 11- 27nm and is in agreement with the crystallite size obtained from XRD analysis.

Table 2. Elemental analysis of $Ni_{0.9}Cd_{0.1}Fe_2O_4$ ferrite sample.

Element present	expected (weight %)	WD-XRF (weight %)
Ni	22.032	23.53
Cd	4.688	3.79
Fe	46.586	45.96
O	26.693	26.70

The stoichiometry of the samples was checked by WD-XRF analysis. The composition of the elements present is given in table 2. From the table it is obvious that the samples show expected stoichiometry; however little cadmium loss is observed which may be due to the volatilization during the sintering process [15].

3.2.Infrared Spectral Study

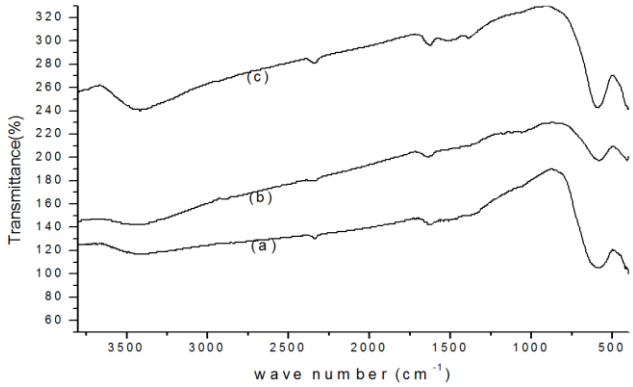

Figure 3 Infrared spectra of $Ni_{0.9}Cd_{0.1}Tb_xFe_{2-x}O_4$ ferrites with (a) x=0.02, (b) x=0.06 and (c) x=0.1.

Figure 3 presents the FTIR spectra of terbium substituted nickel cadmium mixed ferrite samples. As we know, the IR spectra of ferrites are expected to exhibit two major absorption bands in the wave number range 1000- 300cm^{-1}. The higher frequency band (V_1) is usually observed in the range 600- 550cm^{-1}, and is caused by the stretching vibrations of the tetrahedral (A) metal- oxygen bond. The lower one (V_2) is in the range 450- 385cm^{-1}, and is due to the metal- oxygen vibrations in the octahedral (B) sites [16]. These band positions mainly depend on the bond lengths and the nature of the cations involved. The band positions obtained for the studied samples are given in table 3.2 and are found to be in agreement with the reported values [17, 18]. It can be seen from the table that for terbium doping, frequency band position V_1 slightly increased, while V_2 is decreased. Tb^{3+} ions are expected to occupy the octahedral cites owing to their large ionic radius, which may be the reason for the slight decrease in V_2. Increase in V_1 may be due to the contraction of the unit cell due to terbium doping, producing decrease in tetrahedral cite radius.

3.3. Magnetic properties

Magnetic characterization of the samples was carried out using VSM at room temperature with maximum applied field of 20kOe. Figure 4 shows typical hysteresis

loops of Tb^{+} doped Ni-Cd mixed ferrite system. The saturation magnetization (M_S), coercivity (H_C) and remanence (M_R) of all the samples are presented in table 2. It is observed that M_S is increased by terbium substitution up to x=0.06. Rare earth ions are expected to occupy the octahedral sites of ferrites because of their large size. The magnetic moments of rare earth ions generally originate from localized 4f electrons and these are characterized by lower magnetic ordering temperatures [19]. Therefore their magnetic dipolar orientation exhibit disordered form at room temperature and hence Tb^{3+} ions can be considered as nonmagnetic and make no contribution to the magnetization of doped ferrite at room temperature [20]. The replacement of Fe^{3+} from the octahedral sites by most of the rare earths is reported to decrease the saturation magnetization of ferrites [14, 21, 22]. Hence it can be concluded that, terbium doping leads to a cationic redistribution favouring the magnetization of A or B sub lattice, in Ni-Cd mixed ferrites and this may be the reason for the observed increase in M_S. The observed decrease in M_S for x = 0.1 may be due to the decreased particle size. However a clear picture of the cationic distribution may be available only by a neutron diffraction study. Increase in particle size due to terbium doping may be another reason for the increase in M_S.

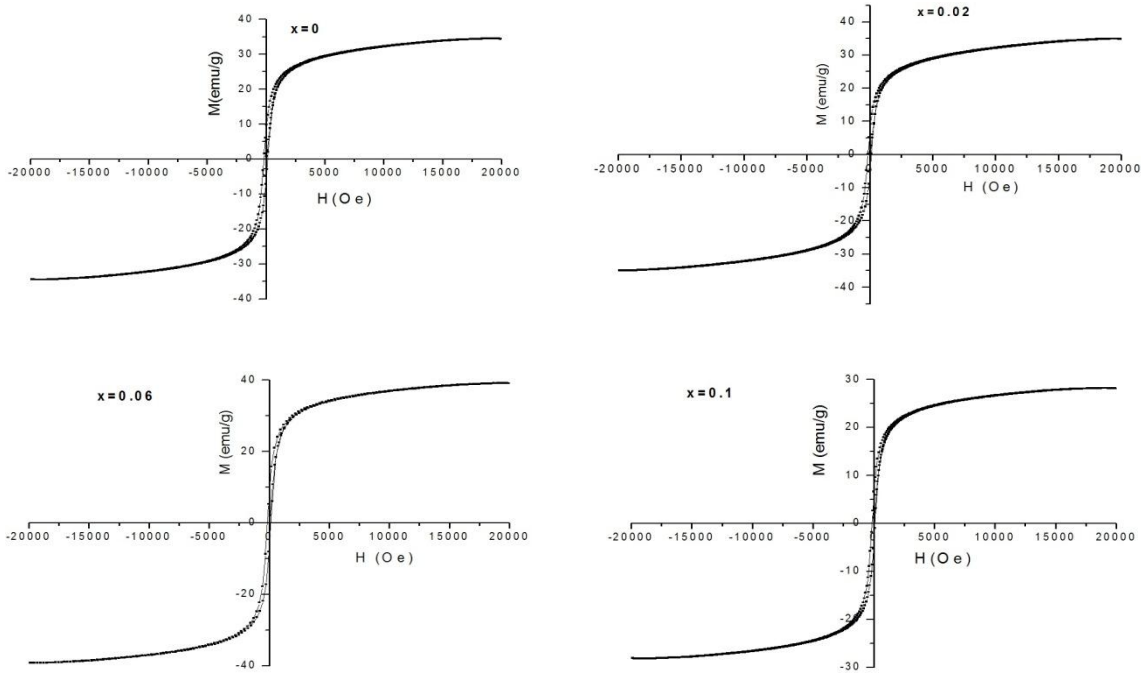

Figure 4 Room temperature hysteresis loops of $Ni_{0.9}Cd_{0.1}Tb_xFe_{2-x}O_4$ ferrites.

Coercivity is observed to decrease in Ni-Cd mixed ferrite by terbium doping. Coercivity depends on defects, strain, presence of nonmagnetic atoms etc. in the material as well as on porosity, particle size and anisotropy. The decrease in H_C may be a result of the increase in particle size in spite of an increase in porosity. It is well known that the coercivity is inversely proportional to the grain size [21,23] . Larger grain size makes the domain wall movement easier and thereby coercivity decreases [19]. Thus increase in magnetization is achieved in Ni-Cd mixed ferrite system by terbium doping.

Table 3 Effect of Tb^{3+} doping on the magnetic parameters and IR frequency band positionss.

Compo-sition (x)	M_S (emu/g)	M_R (emu/g)	H_C (Oe)	V_1 (cm^{-1})	V_2 (cm^{-1})
0.0	34	7.3	165	---	---
0.02	35	5.7	152	586	408
0.06	39	7.5	140	583	407
0.1	28	5.5	126	590	402

3.3. Electrical properties

Variation of dielectric constant with frequency (100Hz to 20MHz) at room temperature is shown in figure 6. It is obvious from the figure that the dielectric constant (ε_r) decreases rapidly with increase in frequency and becomes almost frequency independent at very high frequencies. This is a normal dielectric behaviour of spinel ferrites [24]. Similar results are reported [25 -29]. No change in this behaviour is observed due to terbium doping

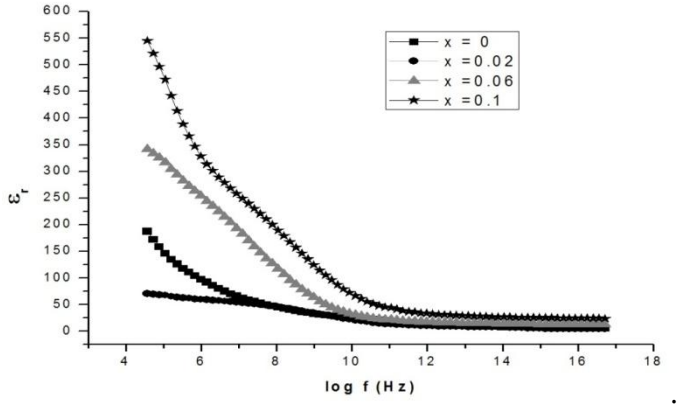

Figure 6 Variation of dielectric constant with frequency for N-Cd-Tb ferrite system

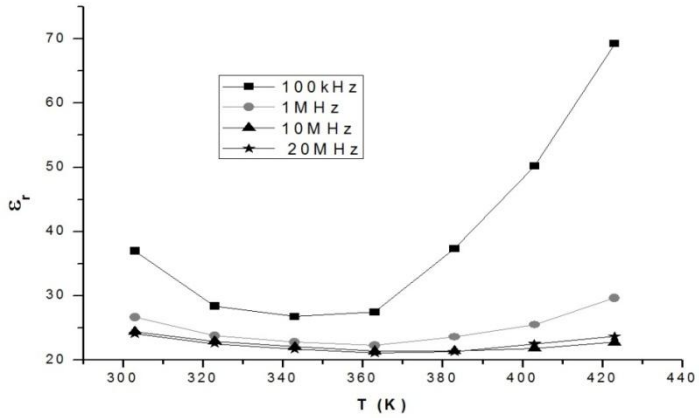

Figure 7 Temperature variation of dielectric constant for the sample with x=0.1 at selected frequencies

Dielectric constant is observed to increase slightly by terbium doping (x=0.02). However, further doping has increased the dielectric constant. This can be understood in terms of the variation of resistivity with terbium content, since dielectric permittivity is directly proportional to the square root of conductivity [30]. Temperature dependence of real part of dielectric permittivity at selected frequencies for the sample with x=0.1 is depicted in figure 7. All other doped compositions exhibit similar behaviour, however the initial decrease in ε_r is absent in the pure nickel ferrite sample. The initial decrease in ε_r indicates the metallic nature of the samples in the low temperature region as a result of terbium doping [31]. The increase in ε_r with increase in temperature can be related to the increase in drift mobility of charge carriers.

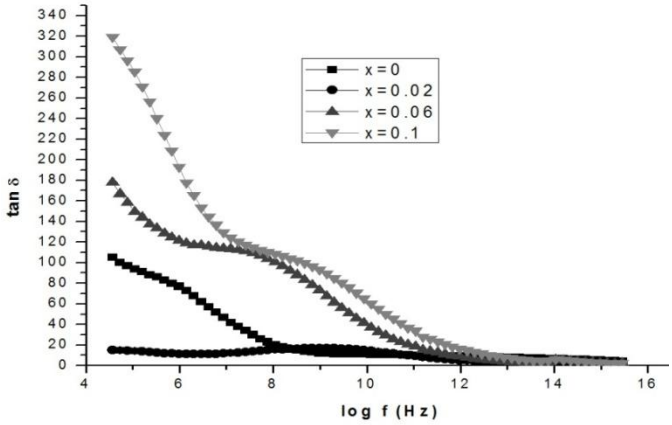

Figure 8. Variation of loss factor with frequency.

Figure 8 shows the variation of loss factor with frequency for the studied terbium doped Ni-Cd nano ferrite samples. The dielectric loss factor $\tan\delta$ represents the energy loss within the

dielectric medium. All the compositions show normal dielectric behaviour and is already explained in the previous chapter. It is obvious from the figure that dielectric loss initially decreases and then increases with increase in Tb^{3+} content and is due to the change in resistivity due to doping [12].

4. *Conclusions*

Fine particles of Ni-Cd-Tb mixed ferrite were prepared by sol-gel method. Terbium substitution resulted in an increase in the particle size and a reduction in the lattice parameter of Ni-Cd mixed ferrite. Magnetic characterization reveals that the saturation magnetization can be enhanced by minor terbium doping and the maximum saturation magnetization is obtained for the sample with x=0.06. Coercivity shows slight decrease by terbium doping. However, terbium doped samples exhibited metallic behaviour at the low temperature region. Dielectric constant of Ni-Cd ferrites is observed to decrease slightly by terbium doping up to x = 0.02 and this may be attributed to the increase in resistance. Hence increased magnetization and slight increase in resistivity is achieved in Ni-Cd ferrites by minor terbium doping. For getting a clear picture of the cationic distribution, which helps in improving the properties, neutron diffraction studies are also to be carried out.

Acknowledgement

BPJ is grateful to The University Grants Commission of India for thefinancial support of this research work. The authors are thankful to STIC CUSAT Cochin and CIF IIT Guwahati for various measurements.

Reference

[1]. Ge-Liang Sun, Jian-Bao Li, Jing-Jing Sun, Xiao-Zhan Yang, J. Magn. Magn. Mater. 281 (2004) 173-177.

[2]. N. Rezlescue, L. Rezlescue, P.D. Popa, J. Magn. Magn. Mater. 194 (2000) 215.

[3]. A. Vasilue, Gh. Maxim, M.L. Crans, Phys. Stat. Sol. A, 13 (1972) 371.

[4]. M.A. Ahmed, E. Ateia, S.I. El-dek, Mater. Lett. 57 (2003) 4256.

[5]. E. Ateia, M.A. Ahmed, A.K. El-Aziz, J. Magn. Magn. Mater. 311 (2007) 545.

[6]. Z. Peng, Xiuli Fu, Huilin Ge, Zhiqiang Fu, C. Wang, L. Qi, H. Miao, J. Magn. Magn. Mater. 323 (2011) 2513-18.

[7]. K. Kamala Bharathi, J.A. Chelvane, G. Markandeyulu, J. Magn. Magn. Mater. 321 (2009) 3677-3680.

[8]. E.E. Sileo, S.E. Jacobo, Physica B 354 (2004) 241-245.

[9]. M.A. Khan, M.U. Islam, M. Ishaque, I.Z. Rahman, A. Genson, S. Hampshire Material Characterization 60 (2009) 73-78.

[10]. B.P. Jacob, S. Thankachan, S. Xavier and E.M. Mohammed, Phys. Scr. 84 (2011) 45702-707.
[11]. S.E. Shirsath, B.G. Toksha, K.M. Jadhav, Mater. Chem. Phys. 117 (2009) 163-168.
[12]. E. Melagiriyappa, H.S. Jayanna, B.K. Chougule, Mater. Chem. Phys. 112 (2008) 68-73.
[13]. R.P. Pant, M. Arora, B. Kaur, V. Kumar, A. Kumar, J. Magn. Magn. Mater. 322 (2010) 3688-91.
[14]. L. Guo, X. Shen, Y. Feng, J. Alloys Compd. 490 (2010) 301-306.
[15]. K.B. Modi, M.K. Rangolia, M.C. Chhantbar, H.H. Joshi, J. Mater. Sci. (2006) 41 7308-7318.
[16]. R.D. Waldron, Phys. Rev. 99 (1955) 1727.
[17]. S.M. Montmayor, L.A. Garcia-Cerda, J.R. Torres-Lubian, O.S.R. Fernandez, J. Sol-Gel Sci. Techn. 42 (2007) 181.
[18]. L.J. Berchmans, R.K. Selvan, P.N. Selvakumar, C.O. Augustin, Mater. Letts. 58 (2004) 1928.
[19]. W.J. Nellis, S. Legvold, Phys. Rev. 180 (1969) 581-590.
[20]. Jiang Jing, Li Liangchao, Xu Feng, Journal of Rare Earths, 25 (2007) 79-83.
[21]. Jiang J, Yang Y M, Li L C, Physica B: Condensed matter, 329 (2007)105-108.
[22]. A.C.F.M. Costa, M.R. Morelli, R.H.G.A. Kiminami, J. Material Science, 39 (2004) 1773-1778.
[23]. S. Mishra, N. Karak, T.K. Kundu, D. Das, N. Maity, D. Chackravorty, Material Letters 60 (2006)1111-1115.
[24]. K.K. Katsmi, S. Mamoru, I. Katsuya, Bull. Chem. Soc. 48 (1975) 1764.
[25]. M.A. El Hiti, J. Magn. Magn. Mater. 192 (1999) 305.
[26]. K.M. Batoo, S. Kumar, C.G. Lee, Alimuddin, Current Applied Physics 9 (2009) 1072-78.
[27]. N. Singh, A. Agarwal, S. Sanghi, Current Applied Physics 11 (2011) 783-789.
[28]. K.K. Bharathi, G. Markandeyulu, J. Appl. Phys. 103 (2008) 07E30941.
[29]. D. Ravinder, K. V. Kumar, P. Balaya, Material Letters 18 (2001) 210-214.
[30]. A.M. Shaikh, S.S. Bellard, B.K. Chougule, J. Magn. Magn. Mater. 195 (1999) 384.
[31]. M.A. Ahmed, Samitha. T. Bishay, G. Abdelatif, J. Phys. Chem. Solids 62 (2001) 1039.